
Long-range Brain Graph Transformer

Shuo Yu^{1,2}, Shan Jin³, Ming Li^{4,5}, Tabinda Sarwar⁶, Feng Xia⁶✉

¹School of Computer Science and Technology, Dalian University of Technology, China

²Key Laboratory of Social Computing and Cognitive Intelligence (Dalian University of Technology),
Ministry of Education, China

³School of Software, Dalian University of Technology, China

⁴Zhejiang Institute of Optoelectronics, China

⁵Zhejiang Key Laboratory of Intelligent Education Technology and Application,
Zhejiang Normal University, China

⁶School of Computing Technologies, RMIT University, Australia

{shuo.yu, f.xia}@ieee.org

jinshan0924@mail.dlut.edu.cn

mingli@zjnu.edu.cn

tabinda.sarwar@rmit.edu.au

Abstract

Understanding communication and information processing among brain regions of interest (ROIs) is highly dependent on long-range connectivity, which plays a crucial role in facilitating diverse functional neural integration across the entire brain. However, previous studies generally focused on the short-range dependencies within brain networks while neglecting the long-range dependencies, limiting an integrated understanding of brain-wide communication. To address this limitation, we propose **Adaptive Long-range aware TransformER (ALTER)**, a brain graph transformer to capture long-range dependencies between brain ROIs utilizing biased random walk. Specifically, we present a novel long-range aware strategy to explicitly capture long-range dependencies between brain ROIs. By guiding the walker towards the next hop with higher correlation value, our strategy simulates the real-world brain-wide communication. Furthermore, by employing the transformer framework, ALTER adaptively integrates both short- and long-range dependencies between brain ROIs, enabling an integrated understanding of multi-level communication across the entire brain. Extensive experiments on ABIDE and ADNI datasets demonstrate that ALTER consistently outperforms generalized state-of-the-art graph learning methods (including SAN, Graphormer, GraphTrans, and LRGNN) and other graph learning based brain network analysis methods (including FBNETGEN, BrainNetGNN, BrainGNN, and BrainNETTF) in neurological disease diagnosis. Cases of long-range dependencies are also presented to further illustrate the effectiveness of ALTER. The implementation is available at <https://github.com/yushuowiki/ALTER>.

1 Introduction

Brain networks represent a blueprint of communication and information processing across different regions of interest (ROIs) Zamani Esfahlani et al. [2022], Seguin et al. [2023]. The interaction between anatomically connected ROIs within brain networks is the foundation of brain network analysis tasks Akarca et al. [2021]. As shown in Figure 1, numerous studies have shown that brain networks exhibit not only short-range connectivity (i.e., short-range dependencies) but also extensive long-range connectivity (i.e., long-range dependencies) Modha and Singh [2010], Arnulfo et al.

[2020], Miura et al. [2022], Jin et al. [2024]. Short-range dependencies rely on the neighbourhood space, whereas long-range dependencies reflect long distance communication among ROIs. Such long-range dependencies play a vital role in theoretical analyses of brain function Deco et al. [2021], dysfunction Harrington and Ginty [2013], organization Li et al. [2020], dynamics Arnulfo et al. [2020], and evolution Paolino et al. [2020]. Therefore, it is necessary to capture long-range dependencies within brain networks to better represent communication connectivity and facilitate brain network analysis tasks to extract valuable insights. The communication connectivity is also known as functional connectivity, representing the interaction between brain ROIs.

Several existing studies have been devoted to representing communication connectivity within brain networks via graph learning methods for network analysis tasks Li et al. [2021], Cui et al. [2023], Yan et al. [2019], Kan et al. [2022b]. However, as previously mentioned, they generally focus on the aggregation of neighborhood information, i.e., short-range dependencies, which still limits their effectiveness by neglecting the crucial long-range dependencies. Most of the studies build models to analyze node (ROIs) features and structures (inter-ROI connectivity) using Graph Neural Networks (GNNs) with message-passing mechanism. The limited expressiveness of GNNs fails to capture the long-range dependencies in brain networks. While the group-based graph pooling operations cluster ROIs, these are still limited to regional similarities and are not sufficient to represent long-range communication connectivities.

To address this limitation of solely considering the short-range dependencies, we aim to develop a solution that leverages long-range dependencies to enhance brain network analysis tasks. Currently, the capturing the long-range dependencies has been addressed in different network analysis tasks outside the scope of brain studies, such as those related to social networks and molecular networks Huang et al. [2019], Gasteiger et al. [2021], Zhou et al. [2023], Ma et al. [2022]. Among these, random walk methods are widely adopted, as they can explicitly capture long-range dependencies

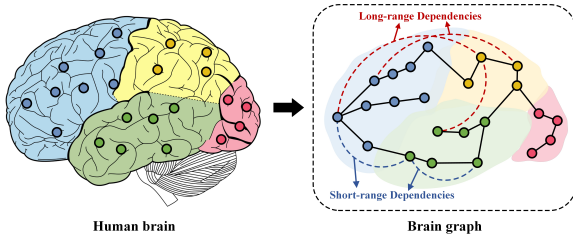


Figure 1: An illustration of long-range dependencies and short-range dependencies within human brain.

by aggregating structure information across the entire random walk sequence Nikolentzos and Vazirgiannis [2020], Xia et al. [2021], Yeh et al. [2023], Jabri et al. [2020]. In conventional random walk methods, the transition probability from a node to one of its neighbors is typically uniform. However, several studies have observed that different pairs of ROIs typically demonstrate varying communication strengths in brain activity, where stronger communication indicates greater dependencies among ROIs Varela et al. [2001], Uhlhaas and Singer [2006], Lutz et al. [2002]. Therefore, employing conventional random walk methods to sample the next hop with uniform probability renders it impossible to capture the long-range dependencies within brain networks.

Based on the above observation, we are dedicated to capturing long-range dependencies in brain networks under the varying communication strengths among ROIs. In this paper, we propose **Adaptive Long-range aware TransformER** (ALTER), a brain graph transformer to capture long-range dependencies between brain ROIs extracted from biased random walk. Specifically, in order to capture long-range dependencies within brain networks, we firstly present an **Adaptive Long-range Aware** (ALGA) strategy based on random walk in Section 3.1, which explicitly samples random walk sequences based on varying communication strengths among ROIs. In this strategy, we initially calculate the inter-ROI correlations as adaptive factors to evaluate their communication strengths. Subsequently, the use of random walk is biased, subject to the next hop with a higher correlation value, thus explicitly encoding long-range dependencies as long-range embeddings through random walk sampling. Furthermore, given the significance of both short-range and long-range dependencies in brain network analysis tasks, we introduce an effective brain graph transformer in Section 3.2, which can capture different levels of communication connectivities in human brains. Specifically, we inject the long-range embeddings into a transformer framework and integrate both short-range and long-range dependencies between ROIs using the self-attention mechanism.

The contributions of the paper are summarized as follows: 1) pioneering the explicit emphasis on the significance and challenges of capturing long-range dependencies in brain network analysis tasks, we

propose a novel solution for capturing long-range dependencies within brain networks; 2) to address the limitations of previous studies that overlook long-range dependencies within brain networks, we introduce a novel brain graph transformer with adaptive long-range awareness, which leverages the communication strengths between ROIs to guide the capturing of long-range dependencies, enabling an integrated understanding of multi-level communication across the entire brain; 3) extensive experiments on ABIDE and ADNI datasets demonstrate that ALTER consistently outperforms generalized graph learning methods and other graph learning-based brain network analysis methods.

2 Related Work

2.1 Brain Network Analysis

Several studies have developed graph learning-based methods for brain network analysis tasks, such as neurological disease diagnosis and biological sex prediction Li et al. [2021], Yan et al. [2019], Kan et al. [2022b], Kim et al. [2021], Kan et al. [2022a]. The majority of studies have utilized GNNs to learn the information of ROIs and inter-ROI connectivity. For instance, Li et al. Li et al. [2021] utilized GNNs with ROI-aware and ROI-selection to perform community detection while retaining critical nodes. Kan et al. Kan et al. [2022a] dynamically optimized a learnable brain network. Additionally, a few models based on specific graph pooling operations were also proposed to retain the communication information of brain networks. Specifically, Yan et al. Yan et al. [2019] designed group-based graph pooling operations to enable explainable brain network analysis. Kan et al. Kan et al. [2022b] considered the similarity property among brain ROIs and designed a graph pooling function based on clustering. However, these approaches are generally limited to the aggregation of neighborhood information, while neglecting the long-range connectivity that plays a key role in brain network analysis tasks Arnulfo et al. [2020].

2.2 Graph Transformer

Several existing studies have focused on developing the transformer variants for graph representation learning Dwivedi and Bresson [2021], Kreuzer et al. [2021], Ying et al. [2021], Wu et al. [2021], Tao et al. [2024]. Transformers have demonstrated competitive or even superior performance over GNNs. Dwivedi et al. Dwivedi and Bresson [2021] were the first to extend the transformer to graphs, defining the eigenvectors as positional embeddings. Kreuzer et al. Kreuzer et al. [2021] improved the positional embeddings and enhanced the transformer model by learning from the full Laplacian spectrum. Ying et al. Ying et al. [2021] embedded the structural information of graph into a transformer, yielding effective results. Moreover, some studies have applied transformers to address unique issues in general graphs or domain-specific graphs. Wu et al. Wu et al. [2021] utilized global attention to capture long-range dependencies within general graphs. Tao et al. Tao et al. [2024] employed the transformer model to integrate both temporal and spatial information in social networks for disease detection.

3 Method

Within the brain graph, the collection of brain ROIs serves as the node set, and the features of these ROIs serve as the node features. The connectivity among brain ROIs is generally represented by the adjacency matrix. In this paper, we focus on analyzing these brain graphs for neurological disease diagnosis. Formally, consider a set of subjects' brain network $\{G_1 \dots G_L\} \subseteq \mathcal{G}$ and their disease state labels $\{y_1 \dots y_L\} \subseteq Y$, where L is the total number of individuals (size of the dataset). Each brain graph G contains N ROIs, defined as $G = (V, X, A)$, where V is node set, $X \in \mathbb{R}^{N \times d}$ are node features with dimension d , and $A \in \mathbb{R}^{N \times N}$ is an adjacency matrix. We aim to learn a representation vector h_G that will allow us to predict the disease state of brain graph G , i.e., $y_G = f(h_G)$ where f is prediction function. Notably, the proposed method can also deal with other brain network analysis tasks such as biological sex prediction.

The overall framework of ALTER is illustrated in Figure 2. Briefly, we first extract the node features X_G and adjacency matrix A_G from the fMRI data. Subsequently, adaptive factors F_G are calculated using the temporal features of the fMRI data. Next, using the adaptive factors F_G and the adjacency matrix A_G , the long-range embedding E_G representing the long-range dependencies

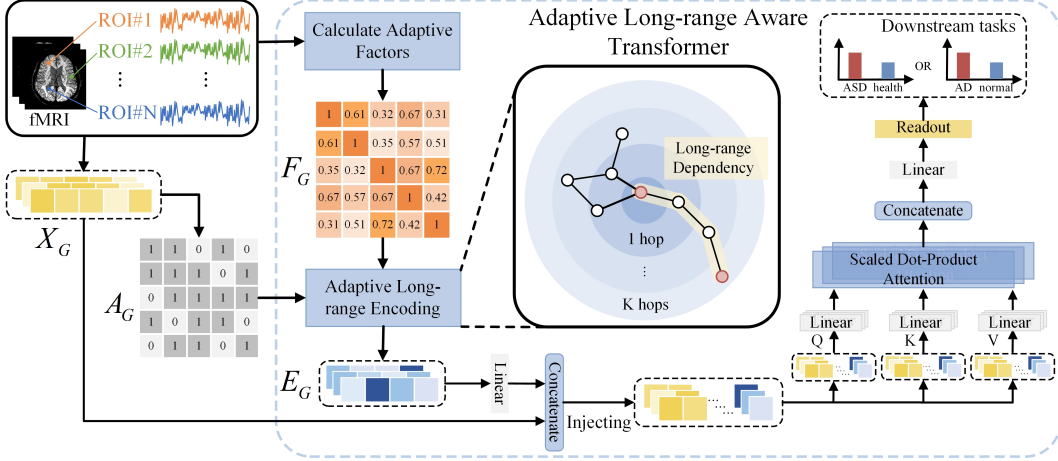


Figure 2: The overall framework of the proposed ALTER.

is obtained through adaptive long-range encoding. The encoding is utilized by our **Adaptive Long-range Aware (ALGA)** strategy to explicitly encapsulate the long-range dependencies among ROIs as long-range embedding E_G . Finally, the long-range embedding E_G is injected into the self-attention module, and a graph-level representation of the brain network is generated using the readout function to the downstream tasks. The complete training process is supervised by the cross-entropy loss.

Detailed description of these steps are discussed in the upcoming sections.

3.1 Adaptive Long-range Aware (ALGA) Strategy

As previously mentioned, previous studies primarily focus on aggregating information from neighboring ROIs, generally neglecting their long-range connectivity. In light of this, our goal is to design an efficient strategy to capture long-range dependencies among the ROIs. We now explain how the adaptive long-range aware strategy achieves this through the computation of adaptive factors and the adaptive long-range encoding.

3.1.1 Adaptive Factors

The correlation between ROIs reflects their communication strength within specific time frames, which is crucial for comprehending the functional organization, dysfunctions, and information propagation in the brain Seguin et al. [2023], Fell and Axmacher [2011]. Neuroscientific investigations have unveiled the existence of phase synchrony in neural oscillations among distinct ROIs, closely associated with the occurrence of perceptual motor behaviors and the integration of brain functional organization Varela et al. [2001], Uhlhaas and Singer [2006], Lutz et al. [2002]. The degree of phase synchrony indicates the strength of connectivity between ROIs, whereby higher phase synchrony signifies stronger communication and consequently higher correlation values among the respective ROIs. This manner simulates real-world brain-wide communication.

Considering the above observation, we first calculate the correlation between ROIs as adaptive factors $F_G \in \mathbb{R}^{N \times N}$ to evaluate the communication strengths between ROIs. Specifically, the adaptive factor f_{ij} , denoting the communication strength between node i and node j within the brain graph G , is defined as:

$$f_{ij} = \begin{cases} \frac{\text{Cov}(t_i, t_j)}{\sigma(t_i)\sigma(t_j)}, & \text{if } v_i \text{ and } v_j \text{ are connected,} \\ 1, & \text{if } i = j, \\ 0, & \text{otherwise,} \end{cases} \quad (1)$$

where t_* denotes the raw feature of the brain ROI v_* (e.g., temporal feature of fMRI data). $\text{Cov}(\cdot)$ and $\sigma(\cdot)$ denote covariance and variance operations, respectively. The adaptive factors F_G will influence the exploration mechanism of the random walk in the adaptive long-range encoding (Section 3.1.2). Specifically, ROIs with stronger connectivities exhibit higher transfer probabilities of the next hop

compared to ROIs with weaker connectivities in the random walk. Note that for simplicity, we choose Pearson correlation coefficient to define the adaptive factors, without any modification.

3.1.2 Adaptive Long-range Encoding

The adaptive factors between ROIs, computed in the preceding step, are crucial for effectively capturing long-range dependencies between brain ROIs. Motivated by the random walk methods Huang et al. [2019], Gasteiger et al. [2021], Xia et al. [2020], we approach the problem of capturing long-range dependencies as a structural encoding task. By sampling and encoding node sequences into embeddings, we effectively capture long-range communication between brain ROIs. Hence, we compute a long-range embedding using the walker sampling of node sequences under the constraint of adaptive factors.

In a network, a random walk involves transitioning from one node to another. Specifically, when a walker moves from node i , the probability of the walker moving to node j in the next step depends solely on the conditions of nodes i and j . This characteristic, where the probability of reaching node j is independent of the preceding step at node i , defines a Markov process. Thus, the random walk process inherently embodies a Markovian nature.

Let p_{ij} represent the probability that the walker walks from node i to node j in brain graph G , then p_{ij} can be represented in the following matrix form:

$$P_G = \begin{bmatrix} p_{11} & \cdots & p_{1n} \\ \cdots & \cdots & \cdots \\ p_{n1} & \cdots & p_{nn} \end{bmatrix}, 0 \leq p_{ij} \leq 1, \sum_{v=1}^n p_{ij} = 1, \quad (2)$$

where matrix P_G is the transfer matrix of brain graph G . Then the state vector is defined as:

$$T(k) = (t_1(k), t_2(k), \dots, t_n(k)), \sum_{j=1}^n t_j(k) = 1, \quad (3)$$

where k is denoted as the number of hops in random walks. $t_j(k)$ is the probability of the walker stops at node j after k times walk. $t_j(k)$ is called k steps state probability. According to the total probability formula, we get:

$$t_i(k+1) = \sum_{j=1}^n t_j(k) p_{ij}, k = 0, 1, 2, \dots, K. \quad (4)$$

where K represents the total number of hops in random walk. So, we get the general recursive formula as $T(k) = T(0) P_G^k$. Nevertheless, brain networks deviate from general networks as pairwise ROIs typically exhibit distinct communication strengths, indicative of the collaborative nature of ROIs in brain activity. Falsely treating pairs of ROIs with varying communication strengths equally may disrupt the collaborative dynamics within brain activity. Given this fact, the transfer probability of the walker in a brain network can be fine-tuned using the adaptive factors, i.e., $\hat{P}_G = F_G \odot P_G$, where \odot denotes the dot product operation. Formally, considering the adjacency matrix A_G and the corresponding diagonal degree matrix D_G of a brain graph G , along with the obtained adaptive factors F_G , we define the random walk kernel R for adaptive long-range encoding as follows:

$$R = (F_G \odot A_G) D_G^{-1}. \quad (5)$$

In particular, The introduction of degree matrix can help to obtain richer information about brain-wide communication and is very commonly used in network analytics Dwivedi et al. [2022]. Since the degree matrix provides the number of degrees for each ROI, its ability to reflect the active state of the ROI in communication is important in determining which ROIs play a key role in information propagation. Hence, a degree matrix determines the transfer probability of a node to its neighboring nodes and highly influences the behavior of walker Bera and Seshadhri [2020].

In the K -step random walk, the long-range embedding E_G initialized by the adaptive long-range encoding is defined as:

$$e_i = [I, R, R^2, \dots, R^{K-1}]_{ii} \in \mathbb{R}^K, \quad (6)$$

where I denotes the identity matrix. e_i denotes a long-range embedding associated with the i -th node, encapsulating the long-range dependency associated with i -th node. Through adaptive long-range encoding, we can explicitly capture long-range dependencies among ROIs in the brain graph G and encode them into the form of long-range embeddings E_G .

3.2 Long-range Brain Graph Transformer

In Section 3.1.2, we obtained the long-range embedding E_G that explicitly encode the long-range connectivities within the brain network G . As short-range dependencies are also significant, we aim to present an effective brain graph transformer by first injecting long-range embeddings into brain network representation learning and then integrate both long-range and short-range dependencies for learning a more comprehensive representation. To achieve this objective, we begin by describing the process of injecting long-range embeddings E_G into the brain graph transformer. Later, we explain how the self-attention mechanism can be utilized to integrate long-range and short-range dependencies among brain ROIs.

Injecting Long-range Embedding. The computed long-range embeddings E_G should be injected into the brain network transformer in a manner that enhances its utility. To achieve this, we introduce a fine-tuning procedure aimed at enhancing long-range embeddings E_G and injecting them into the brain graph transformer. Specifically, we utilize a linear layer as a remapping function for long-range embeddings E_G , facilitating the injection of long-range dependencies within the brain network. This process enables the acquisition of trainable long-range embeddings \hat{E}_G with dimension k' . Formally, this procedure is defined as:

$$\hat{E}_G = \text{LL}(E_G; W_G) = W_G E_G + b_G \in \mathbb{R}^{N \times k'}, \quad (7)$$

where $W_G \in \mathbb{R}^{k' \times k}$ and $b_G \in \mathbb{R}^{k'}$ denote learnable weight matrix and bias vector, respectively.

Self-attention Module. Transformer-based models generally surpass conventional representation learning methods in their ability to capture pairwise token correlations and the influence of individual tokens. This stems from the self-attention mechanism's capability to allow inter-token communication. Nonetheless, employing initial node features as input tokens is insufficient for Transformer-based models to effectively capture complex inter-dependencies within brain networks. Furthermore, pairwise ROIs often exhibit varying degrees of short- and long-range dependencies across various brain network analysis tasks Pinho et al. [2023], Roy et al. [2022], Bucsea et al. [2023], Chen et al. [2023]. Hence, we need to integrate both long-range and short-range communication among ROIs through a self-attention module. To model this mechanism, we begin by constructing tokens through the combination of learnable long-range embeddings \hat{E}_G and initial node features X_G . Then, we utilize a vanilla transformer encoder as the framework for the self-attention module.

Formally, we concatenate learnable long-range embeddings \hat{E}_G and initial node features X_G as tokens \hat{X}_G , and then utilize a transformer encoder with L -layer nonlinear mapping and M attention head to learn comprehensive node features Z_G :

$$\hat{X}_G = [X_G | \hat{E}_G] \in \mathbb{R}^{N \times (d+k')}, \quad (8)$$

$$Z_G = W_o \left(\parallel_{m=1}^M Z_G^{m,l} \right) \in \mathbb{R}^{N \times d_{out}}, \quad Z_G^{m,l} = \text{softmax} \left(\frac{Q^{m,l} K^{m,lT}}{\sqrt{d_{out}^{m,l}}} \right) V^{m,l} \in \mathbb{R}^{N \times d_{out}^{m,l}}, \quad (9)$$

with $Q^{m,l} = W_q Z_G^{m,l-1}$, $K^{m,lT} = (W_k Z_G^{m,l-1})^T$, and $V^{m,l} = W_v Z_G^{m,l-1}$ are the query matrix, the key matrix, and the value matrix, where $Z_G^0 = \hat{X}_G$, \parallel and $[\cdot | \cdot]$ both indicate the concatenate operation, l and m denote the layer index and the head index, $W_q, W_k, W_v \in \mathbb{R}^{d_{out}^{m,l} \times d_{out}^{m,l-1}}$ and $W_o \in \mathbb{R}^{d_{out} \times d_{out}^m}$ are learnable projection matrices. In the representation learning procedure, the employed Transformer framework enables the learned Z_G to integrate both short-range and long-range dependencies between brain ROIs by introducing long-range embedding. This design allows our method to adaptively represent the communication connectivities in human brains.

Readout Module. To accomplish brain network analysis tasks, we take the output Z_G of the self-attention module as the criterion, and then utilize an efficient readout function to derive the entire brain graph representation to further enhance the performance. In addition, we train an additional classifier for downstream tasks. The final classification basis is obtained as follows:

$$Y_G = \text{Softmax}(\text{MLP}(\text{Readout}(Z_G))). \quad (10)$$

In Section 4.2, we evaluate the performance of various pooling methods. Ultimately, we employ clustering-based pooling as the readout function in the proposed method.

4 Experiments

In this section, we analyzed the following aspects to demonstrate the effectiveness of the proposed method and its capability to capture long-range dependencies within brain networks.

Q1. Does ALTER outperform other state-of-the-art models?

Q2. How does the proposed adaptive long-range aware strategy perform in different model architectures accompanied by various readout functions?

Q3. Does ALTER capture long-range dependencies within brain networks, and is ALGA strategy considered a key component?

4.1 Experimental Settings

Datasets and Preprocessing. We evaluate the proposed method using two brain network analysis-related fMRI datasets. 1) *Autism Brain Imaging Data Exchange (ABIDE)*¹, which contains 519 Autism spectrum disorder (ASD) samples and 493 normal controls. 2) *Alzheimer’s Disease Neuroimaging Initiative (ADNI)*², which contains 54 Alzheimer’s disease (AD) samples and 76 normal controls. During the construction of the brain graph, we first preprocess the fMRI data using the Data Processing Assistant for Resting-State Function (DPARSF) MRI toolkit. Next, we define brain ROIs based on predefined atlases from preprocessed fMRI data and calculate the average time-series feature for individual brain ROI. Finally, we formalize the brain graph $G = (V, X, A)$ for each sample according to the average time-series features of brain ROIs. Specifically, node features X are functional connectivity matrix calculated by Pearson correlation, the adjacency matrix A is the thresholded functional connectivity matrix to generate binary matrix of 0s or 1s, where the threshold is 0.3. The details of datasets and preprocessing can be found in Appendix A.

Baselines. The selected baselines correspond to two categories. The first category is generalized graph learning methods (Generalized - not specifies to brain networks), including SAN Kreuzer et al. [2021], Graphormer Ying et al. [2021], GraphTrans Wu et al. [2021], and LRGNN Wei et al. [2023]. The second category (Specialized) is the brain graph-based methods, including BrainNetGNN Kan et al. [2022b], FBNETGEN Kan et al. [2022a], BrainGNN Li et al. [2021], BrainNETTF Kan et al. [2022b], A-GCL Zhang et al. [2023], and ContrastPool Xu et al. [2024]. Note that the original code shared by the authors of these baselines is used for the comparative analysis. Please refer to the Appendix A for the details.

Metrics. Given the medical application of neurological disease classification tasks, we utilize both machine learning and medical diagnostic-specific metrics to evaluate the performance of the proposed method. These include classification Accuracy (ACC), Area Under the Receiver Operating Characteristic Curve (AUC), F1-Score, Sensitivity (SEN), and Specificity (SPE). In the experimental results, we report the mean and standard deviation across 10 random runs on the test dataset.

Implementation Details. In the proposed method, we set the number of steps K for adaptive random walk to 16. The number of nonlinear mapping layers L and attention heads M of the self-attention module are set to 2 and 4, respectively. For all datasets, we randomly divide the training set, evaluation set and test set by the ratio of 7 : 1 : 2. In the train processing, we adopt Adam as optimizer and CosLR as scheduler by a initial learning rate of 10^{-4} and a weight decay of 10^{-4} . The batch size is set to 16 and the epoch is set to 200. All experiments are implemented using the PyTorch framework, and computations are performed on one Tesla V100.

4.2 Performance Comparison

In this sections, we evaluate the performance of ALTER by comparison with existing baselines to address **Q1**.

¹<http://preprocessed-connectomes-project.org/abide/>

²<https://adni.loni.usc.edu/>

Table 1: Performance comparison with two categories of baselines on the two chosen datasets (%). The best results are marked in bold and the standard deviations are in parentheses.

| Category | Method | ABIDE | | | | ADNI | | | |
|-------------|--------------|-------------------|-------------------|--------------------|-------------------|-------------------|-------------------|-------------------|--------------------|
| | | AUC | ACC | SEN | SPE | AUC | ACC | SEN | SPE |
| Generalized | SAN | 71.3 (2.1) | 65.3 (2.9) | 55.4 (9.2) | 68.3 (7.5) | 68.1 (3.4) | 62.6 (5.2) | 52.4 (6.2) | 63.3 (8.5) |
| | Graphormer | 63.5 (3.7) | 60.8 (2.7) | 78.7 (22.3) | 36.7 (23.5) | 60.6 (5.2) | 55.7 (3.1) | 60.1 (11.3) | 47.7 (13.5) |
| | GraphTrans | 60.1 (6.7) | 57.8 (4.7) | 65.7 (10.3) | 49.7 (11.5) | 61.2 (3.7) | 58.3 (5.1) | 66.2 (7.2) | 49.3 (3.1) |
| | LRGNN | 70.3 (4.1) | 66.1 (2.5) | 58.4 (9.2) | 65.2 (6.8) | 71.5 (6.4) | 67.3 (2.1) | 59.6 (1.2) | 49.7 (2.3) |
| Specialized | FBNETGEN | 75.6 (1.2) | 68.0 (1.4) | 64.7 (8.7) | 62.4 (9.2) | 73.5 (3.9) | 65.0 (2.6) | 61.3 (2.1) | 59.7 (1.2) |
| | BrainNetGNN | 55.3 (1.9) | 51.2 (5.4) | 67.7 (37.5) | 33.9 (34.2) | 53.7 (7.2) | 50.1 (2.1) | 64.2 (6.8) | 43.8 (8.0) |
| | BrainGNN | 71.6 (1.6) | 75.1 (3.2) | 69.4 (5.2) | 63.4 (7.1) | 63.5 (2.5) | 61.5 (3.2) | 65.1 (3.4) | 53.5 (4.1) |
| | BrainNETTF | 80.2 (1.0) | 71.0 (1.2) | 72.5 (5.2) | 69.3 (6.5) | 76.5 (2.4) | 69.0 (2.7) | 64.7 (7.1) | 75.0 (8.1) |
| | A-GCL | 53.8 (0.5) | 53.8 (0.6) | 62.3 (5.0) | 54.5 (6.3) | 57.2 (1.1) | 52.2 (0.8) | 57.6 (42.4) | 52.6 (38.2) |
| | ContrastPool | 57.3 (0.8) | 57.4 (0.6) | 57.6 (6.8) | 57.0 (7.7) | 68.5 (3.2) | 69.2 (3.9) | 61.5 (17.2) | 75.4 (21.3) |
| Ours | ALTER | 82.8 (1.1) | 77.0 (1.0) | 77.4 (3.4) | 76.6 (4.6) | 78.8 (2.1) | 74.1 (2.5) | 76.5 (6.1) | 70.0 (6.5) |

Results. Table 1 reports the comparison results between the proposed and the baseline methods. ALTER is able to significantly outperform the two categories of baseline methods for both datasets. In comparison to generalized graph learning methods, the proposed ALTER exhibits a significant improvement in terms of the ACC metric (10.9% improvement on the ABIDE dataset and 6.8% improvement on the ADNI dataset). For the case specialized graph learning methods, we again demonstrated superiority on both datasets in terms of the ACC metric (6.0% improvement on the ABIDE dataset and 5.1% improvement on the ADNI dataset). The reason for this performance improvement is that our method takes into account the communication strengths among brain ROIs and utilizes this characteristic to guide the capture of long-range dependencies within the brain network.

Vairous Readout Function. In the experimental setups with and without the ALGA strategy, we compare the results of ALTER using various readout functions, including max pooling, sum pooling, average pooling, sort pooling Zhang et al. [2018], and clustering-based pooling Kan et al. [2022b]. As illustrated in Table 2 and Figure 3(a), our method employing the ALGA strategy consistently achieved superior performance across all readout function settings. Particularly, the combination of clustering-based pooling and the ALGA strategy yielded the best results. This phenomenon also addresses Q2.

4.3 Ablation Study

In order to assess the performance of the model from the Q2 perspective, we conduct ablation studies on the ALGA strategy. This included performing evaluations with different architectures and readout functions.

Adaptive Long-range Aware with Varying Architectures. To verify the generalisability and effectiveness of the ALGA strategy, we implement it within different architectures, including SAN and Graphormer on the two selected datasets. As shown in Table 2, we find that the ALGA strategy can be adapted to different architectures, where this adaptation effectively improves the predictive power of models. This result demonstrates the effectiveness of this strategy in capturing long-range dependencies within brain networks. It should be noted that this analysis could only be performed on the generalized graph learning methods.

Table 2: Performance comparison with varying architectures on the two chosen datasets (%). The best results are indicated by underlining and the standard deviations are in parentheses.

| Method | ABIDE | | | | ADNI | | | |
|-----------------|-------------------|-------------------|--------------------|--------------------|-------------------|-------------------|-------------------|-------------------|
| | AUC | ACC | SEN | SPE | AUC | ACC | SEN | SPE |
| Graphormer | 63.5 (3.7) | 60.8 (2.7) | 78.7 (22.3) | 36.7 (23.5) | 60.6 (5.2) | 55.7 (3.1) | 60.1 (11.3) | 47.7 (13.5) |
| Graphormer+ALGA | <u>67.2 (2.5)</u> | <u>64.1 (1.9)</u> | <u>82.3 (10.3)</u> | <u>45.9 (12.7)</u> | <u>62.9 (4.1)</u> | <u>60.5 (2.9)</u> | <u>63.5 (4.1)</u> | <u>65.4 (2.9)</u> |
| SAN | 71.3 (2.1) | 65.3 (2.9) | 55.4 (9.2) | 68.3 (7.5) | 68.1 (3.4) | 62.6 (5.2) | 52.4 (6.2) | 63.3 (8.5) |
| SAN +ALGA | <u>72.5 (1.9)</u> | <u>67.8 (3.1)</u> | <u>58.9 (6.5)</u> | <u>70.8 (4.1)</u> | <u>70.1 (2.3)</u> | <u>65.8 (3.7)</u> | <u>55.9 (4.8)</u> | <u>68.3 (6.2)</u> |
| ALTER w/o ALGA | 80.2 (1.0) | 71.0 (1.2) | 72.5 (5.2) | 69.3 (6.5) | 76.5 (2.4) | 69.0 (2.7) | 64.7 (7.1) | 75.0 (8.1) |
| ALTER | <u>82.8 (1.1)</u> | <u>77.0 (1.0)</u> | <u>77.4 (3.4)</u> | <u>76.6 (4.6)</u> | <u>78.8 (2.1)</u> | <u>74.1 (2.5)</u> | <u>76.5 (6.1)</u> | <u>70.0 (6.5)</u> |

Adaptive Long-range Aware with Varying Readout Functions. To further demonstrate that the ALGA strategy plays a key role in the proposed method, we take the ABIDE dataset as a benchmark and attempt to vary the readout function under varying architectures (only the AUC metric is shown, the full result can be referred to the Appendix A). Specifically, we first take the proposed method, SAN, and Graphormer as the basic framework, then employ five approaches including max pooling, sum pooling, average pooling, sort pooling, and clustering-based pooling as the readout functions. This analysis will reveal the prediction ability of the frameworks with varying readout functions in the presence and absence of ALGA strategy. The results of different readout functions under various architectures are shown in Figure 3. We observe that, for any arbitrary readout function, the ALGA strategy enhances the performance of downstream tasks for various architectures compared to those without ALGA.

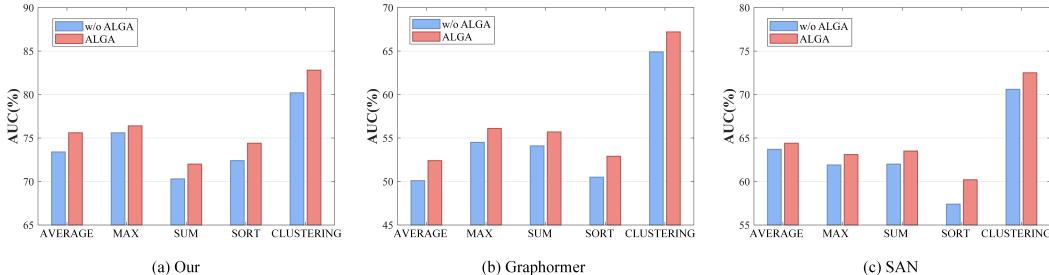


Figure 3: Performance comparison with varying readout functions (%).

4.4 In-depth Analysis of ALTER and ALGA Strategy

Here, we delve into the analysis of ALGA strategy and present cases to evaluate long-range dependencies to demonstrate the effectiveness of ALTER to assess **Q3**.

First, we investigate the impact of key hyperparameter of ALGA strategy of ALTER, which is the number of hops. In this experiment, we set the number of hops of ALGA to 2, 4, 8, 16, 32 for both selected datasets (only the AUC is shown here, the full result can be found in Appendix A). Figure 4(a) clearly shows that for both datasets, the predictive power of the proposed method generally increases as the number of hops increases. This phenomenon can be attributed to the presence of long-range connectivity in communication and information processing within human brains, which our model effectively captures. Ignoring this characteristic will adversely affect the predictive power of graph learning methods in brain network analysis tasks.

Next, we investigate the impact of the adaptive factors in the ALGA strategy. Specifically, we remove the adaptive factors and observe the change in the predictive ability of the proposed method. The experimental results demonstrate (Figure 4(a)) the performance of the proposed method is degraded when adaptive factors are not used to adjust the adaptive long-range encoding. The underlying reason for this result is that inter-ROI correlations play a crucial role in reflecting the communication strengths among brain ROIs. Treating pairwise ROI connectivity equally could potentially have a detrimental effect on brain network analysis tasks that depend on inter-ROI communication.

Finally, we present the cases to demonstrate ALTER’s ability to capture long-range dependencies within brain networks. In this experiment, we randomly sample an example brain graph from the ABIDE test set and used it to train our model to learn the corresponding node features without pooling operation, and thus compute the attention scores among the node features. Figure 4(c) illustrates one example graph and the corresponding attention heatmap (Figure 4(b)). More sample-level and group-level examples can be found in Appendix A. The attention heatmap demonstrates the communication patterns necessary for brain network analysis tasks. Specifically, certain ROIs receive higher attention scores from multiple other ROIs, irrespective of the distance between them. In particular, ROI 6 and ROI 19 present higher attention score, despite the fact that these two ROIs are 5 hops apart (Figure 4(c)).

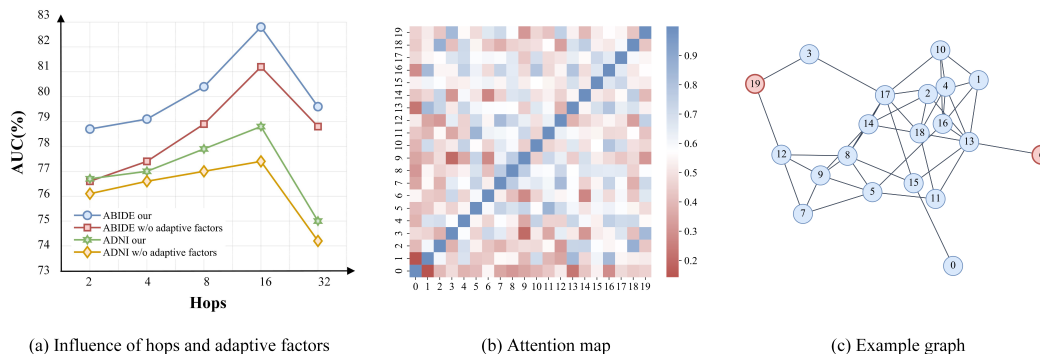


Figure 4: In-depth analysis of ALTER and adaptive long-range aware strategy.

5 Discussions and Conclusion

Limitations. On one hand, while utilizing the brain graph transformer to integrate both short-range and long-range dependencies among brain ROIs, we still cannot ensure an optimal balance between them. In future research, we will explore how to achieve a better balance between short-range and long-range dependencies in brain network analysis, with the aim of achieving better research results. On the other hand, the experimental data we currently employ is limited to fMRI data. Although utilizing these data can demonstrate the crucial role of long-range dependencies in brain network analysis tasks, other forms of data, such as DTI data, are also worthy of exploration. In future work, we will delve into alternative forms of data and propose corresponding methods for capturing long-range dependencies within brain networks.

Conclusion. In summary, we present the ALTER model for brain network analysis, a novel brain graph transformer that explicitly captures long-range dependencies in brain networks and adaptively integrates them with short-range dependencies. Extensive experiments on ABIDE and ADNI datasets demonstrate that ALTER consistently outperforms generalized and specialized (specific to brain network analysis method) graph learning methods. This study presents an initial attempt to capture long-distance dependencies within brain networks and provides a new insight into understanding brain-wide communication and information processing.

Acknowledgments and Disclosure of Funding

This work is supported by the National Natural Science Foundation of China (No.U21A20473, No. 62172370) and the Jinhua Science and Technology Plan (No. 2023-3-003a). Thanks to Guangqing Bai and Yuelong Huang for their help with baselines during rebuttal.

References

- Danyal Akarca, Petra E. Vértes, Edward T. Bullmore, Kate Baker, and Susan E. Gathercole. A generative network model of neurodevelopmental diversity in structural brain organization. *Nature Communications*, 12(1):4216, 2021.
- G. Arnulfo, S. H. Wang, V. Myrov, B. Toselli, J. Hirvonen, M. M. Fato, L. Nobili, F. Cardinale, A. Rubino, A. Zhigalov, S. Palva, and J. M. Palva. Long-range phase synchronization of high-frequency oscillations in human cortex. *Nature Communications*, 11(1):5363, 2020.
- Suman K. Bera and C. Seshadhri. How to count triangles, without seeing the whole graph. In *Proceedings of the 26th ACM SIGKDD International Conference on Knowledge Discovery & Data Mining*, page 306–316, 2020.
- Oana Bucsea, Mohammed Rupawala, Ilana Shiff, Xiaogang Wang, Judith Meek, Maria Fitzgerald, Lorenzo Fabrizi, Rebecca Pillai Riddell, and Laura Jones. Clinical thresholds in pain-related facial activity linked to differences in cortical network activation in neonates. *PAIN*, 164(5), 2023.
- Weiyi Chen, Oliver Mehlkop, Alexandra Scharn, Hendrik Nolte, Paul Klemm, Sinika Henschke, Lukas Steuernagel, Tamara Sotelo-Hitschfeld, Ecem Kaya, Claudia Maria Wunderlich, Thomas

- Langer, Natalia L. Kononenko, Giavalisco Patrick, and Jens Claus Brüning. Nutrient-sensing agrp neurons relay control of liver autophagy during energy deprivation. *Cell Metabolism*, 35(5): 786–806.e13, 2023.
- Hejie Cui, Wei Dai, Yanqiao Zhu, Xuan Kan, Antonio Aodong Chen Gu, Joshua Lukemire, Liang Zhan, Lifang He, Ying Guo, and Carl Yang. BrainGB: A benchmark for brain network analysis with graph neural networks. *IEEE Transactions on Medical Imaging*, 42(2):493–506, 2023.
- Gustavo Deco, Yonathan Sanz Perl, Peter Vuust, Enzo Tagliazucchi, Henry Kennedy, and Morten L Kringelbach. Rare long-range cortical connections enhance human information processing. *Current Biology*, 31(20):4436–4448, 2021.
- Vijay Prakash Dwivedi and Xavier Bresson. A generalization of transformer networks to graphs. In *Proceedings of the AAAI Workshop on Deep Learning on Graphs: Methods and Applications*, pages 1–8, 2021.
- Vijay Prakash Dwivedi, Anh Tuan Luu, Thomas Laurent, Yoshua Bengio, and Xavier Bresson. Graph neural networks with learnable structural and positional representations. In *Proceedings of the 10th International Conference on Learning Representations*, 2022.
- Juergen Fell and Nikolai Axmacher. The role of phase synchronization in memory processes. *Nature Reviews Neuroscience*, 12(2):105–118, 2011.
- Johannes Gasteiger, Chandan Yeshwanth, and Stephan Günnemann. Directional message passing on molecular graphs via synthetic coordinates. In *Proceedings of the 35th Neural Information Processing Systems*, volume 34, pages 15421–15433, 2021.
- Anthony W. Harrington and David D. Ginty. Long-distance retrograde neurotrophic factor signalling in neurons. *Nature Reviews Neuroscience*, 14(3):177–187, 2013.
- Xiao Huang, Qingquan Song, Yuening Li, and Xia Hu. Graph recurrent networks with attributed random walks. In *Proceedings of the 25th ACM SIGKDD International Conference on Knowledge Discovery & Data Mining*, page 732–740, 2019.
- Allan Jabri, Andrew Owens, and Alexei Efros. Space-time correspondence as a contrastive random walk. In *Proceedings of the 34th Neural Information Processing Systems*, pages 19545–19560, 2020.
- Ming Jin, Changde Du, Huiguang He, Ting Cai, and Jinpeng Li. Pgcn: Pyramidal graph convolutional network for eeg emotion recognition. *IEEE Transactions on Multimedia*, pages 1–13, 2024.
- Xuan Kan, Hejie Cui, Joshua Lukemire, Ying Guo, and Carl Yang. FBNETGEN: Task-aware gnn-based fMRI analysis via functional brain network generation. In *Proceedings of the International Conference on Medical Imaging with Deep Learning*, pages 618–637, 2022a.
- Xuan Kan, Wei Dai, Hejie Cui, Zilong Zhang, Ying Guo, and Carl Yang. Brain network transformer. In *Proceedings of the 36th Neural Information Processing Systems*, pages 25586–25599, 2022b.
- Byung-Hoon Kim, Jong Chul Ye, and Jae-Jin Kim. Learning dynamic graph representation of brain connectome with spatio-temporal attention. In *Proceedings of the 35th Neural Information Processing Systems*, pages 4314–4327, 2021.
- Devin Kreuzer, Dominique Beaini, Will Hamilton, Vincent Létourneau, and Prudencio Tossou. Rethinking graph transformers with spectral attention. In *Proceedings of the 35th Neural Information Processing Systems*, pages 21618–21629, 2021.
- Junhua Li, Nitish Thakor, and Anastasios Bezerianos. Brain functional connectivity in unconstrained walking with and without an exoskeleton. *IEEE Transactions on Neural Systems and Rehabilitation Engineering*, 28(3):730–739, 2020. doi: 10.1109/TNSRE.2020.2970015.
- Xiaoxiao Li, Yuan Zhou, Nicha Dvornek, Muhan Zhang, Siyuan Gao, Juntang Zhuang, Dustin Scheinost, Lawrence H. Staib, and James S. Duncan. BrainGNN: Interpretable brain graph neural network for fMRI analysis. *Medical image analysis*, 74:102233, 2021.

- Antoine Lutz, Jean-Philippe Lachaux, Jacques Martinerie, and Francisco J. Varela. Guiding the study of brain dynamics by using first-person data: Synchrony patterns correlate with ongoing conscious states during a simple visual task. *Proceedings of the National Academy of Sciences*, 99(3):1586–1591, 2002.
- Fei Ma, Ping Wang, and Xudong Luo. Random walks on stochastic generalized vicsek fractal networks: Analytic solution and simulations. *IEEE Transactions on Network Science and Engineering*, 9(3):1335–1345, 2022.
- Yuki Miura, Min-Yin Li, Omer Revah, Se-Jin Yoon, Genta Narazaki, and Sergiu P. Paşca. Engineering brain assembloids to interrogate human neural circuits. *Nature Protocols*, 17(1):15–35, 2022.
- Dharmendra S. Modha and Raghavendra Singh. Network architecture of the long-distance pathways in the macaque brain. *Proceedings of the National Academy of Sciences*, 107(30):13485–13490, 2010.
- Giannis Nikolentzos and Michalis Vazirgiannis. Random walk graph neural networks. In *Proceedings of the 34th Neural Information Processing Systems*, pages 16211–16222, 2020.
- Annalisa Paolino, Laura R. Fenlon, Peter Kozulin, Elizabeth Haines, Jonathan W. C. Lim, Linda J. Richards, and Rodrigo Suárez. Differential timing of a conserved transcriptional network underlies divergent cortical projection routes across mammalian brain evolution. *Proceedings of the National Academy of Sciences*, 117(19):10554–10564, 2020.
- Júlia S. Pinho, Vincent Cunliffe, Kyriacos Kareklas, Giovanni Petri, and Rui F. Oliveira. Social and asocial learning in zebrafish are encoded by a shared brain network that is differentially modulated by local activation. *Communications Biology*, 6(1):633, 2023.
- Shangran Qiu, Matthew I. Miller, Prajakta S. Joshi, Joyce C. Lee, Chonghua Xue, Yunruo Ni, Yuwei Wang, Ileana De Anda-Duran, Phillip H. Hwang, Justin A. Cramer, Brigid C. Dwyer, Honglin Hao, Michelle C. Kaku, and et al. Multimodal deep learning for alzheimer’s disease dementia assessment. *Nature Communications*, 13(1):3404, 2022.
- Dheeraj S. Roy, Young-Gyun Park, Minyoung E. Kim, Ying Zhang, Sachie K. Ogawa, Nicholas DiNapoli, Xinyi Gu, Jae H. Cho, Heejin Choi, Lee Kamensky, Jared Martin, Olivia Mosto, Tomomi Aida, Kwanghun Chung, and Susumu Tonegawa. Brain-wide mapping reveals that engrams for a single memory are distributed across multiple brain regions. *Nature Communications*, 13(1):1799, 2022.
- T. Sarwar, Y. Tian, B.T.T. Yeo, K. Ramamohanarao, and A. Zalesky. Structure-function coupling in the human connectome: A machine learning approach. *NeuroImage*, 226:117609, 2021.
- Caio Seguin, Olaf Sporns, and Andrew Zalesky. Brain network communication: concepts, models and applications. *Nature Reviews Neuroscience*, 24(9):557–574, 2023.
- Yongfeng Tao, Minqiang Yang, Huiru Li, Yushan Wu, and Bin Hu. Depmstat: Multimodal spatio-temporal attentional transformer for depression detection. *IEEE Transactions on Knowledge and Data Engineering*, pages 1–12, 2024.
- Peter J Uhlhaas and Wolf Singer. Neural synchrony in brain disorders: Relevance for cognitive dysfunctions and pathophysiology. *Neuron*, 52(1):155–168, 2006.
- Francisco Varela, Jean-Philippe Lachaux, Eugenio Rodriguez, and Jacques Martinerie. The brainweb: Phase synchronization and large-scale integration. *Nature Reviews Neuroscience*, 2(4):229–239, 2001.
- Lanning Wei, Zhiqiang He, Huan Zhao, and Quanming Yao. Search to capture long-range dependency with stacking GNNs for graph classification. In *Proceedings of the ACM Web Conference 2023*, page 588–598, 2023.
- Zhanghao Wu, Paras Jain, Matthew Wright, Azalia Mirhoseini, Joseph E Gonzalez, and Ion Stoica. Representing long-range context for graph neural networks with global attention. In *Proceedings of the 35th Neural Information Processing Systems*, pages 13266–13279, 2021.

- Feng Xia, Jiaying Liu, Hansong Nie, Yonghao Fu, Liangtian Wan, and Xiangjie Kong. Random walks: A review of algorithms and applications. *IEEE Transactions on Emerging Topics in Computational Intelligence*, 4(2):95–107, 2020.
- Feng Xia, Ke Sun, Shuo Yu, Abdul Aziz, Liangtian Wan, Shirui Pan, and Huan Liu. Graph learning: A survey. *IEEE Transactions on Artificial Intelligence*, 2(2):109–127, 2021.
- Jiaying Xu, Qingtian Bian, Xinhang Li, Aihu Zhang, Yiping Ke, Miao Qiao, Wei Zhang, Wei Khang Jeremy Sim, and Balázs Gulyás. Contrastive graph pooling for explainable classification of brain networks. *IEEE Transactions on Medical Imaging*, pages 1–14, 2024.
- Yujun Yan, Jiong Zhu, Marlena Duda, Eric Solarz, Chandra Sripada, and Danai Koutra. GroupINN: Grouping-based interpretable neural network for classification of limited, noisy brain data. In *Proceedings of the 25th ACM SIGKDD International Conference on Knowledge Discovery & Data Mining*, page 772–782, 2019.
- Pei-Kai Yeh, Hsi-Wen Chen, and Ming-Syan Chen. Random walk conformer: Learning graph representation from long and short range. In *Proceedings of the AAAI Conference on Artificial Intelligence*, pages 10936–10944, 2023.
- Chengxuan Ying, Tianle Cai, Shengjie Luo, Shuxin Zheng, Guolin Ke, Di He, Yanming Shen, and Tie-Yan Liu. Do transformers really perform badly for graph representation? In *Proceedings of the 35th Neural Information Processing Systems*, pages 28877–28888, 2021.
- Farnaz Zamani Esfahlani, Joshua Faskowitz, Jonah Slack, Bratislav Mišić, and Richard F. Betzel. Local structure-function relationships in human brain networks across the lifespan. *Nature Communications*, 13(1):2053, 2022.
- Muhan Zhang, Zhicheng Cui, Marion Neumann, and Yixin Chen. An end-to-end deep learning architecture for graph classification. In *Proceedings of the AAAI Conference on Artificial Intelligence*, pages 4438–4445, 2018.
- Shengjie Zhang, Xiang Chen, Xin Shen, Bohan Ren, Ziqi Yu, Haibo Yang, Xi Jiang, Dinggang Shen, Yuan Zhou, and Xiao-Yong Zhang. A-GCL: Adversarial graph contrastive learning for fmri analysis to diagnose neurodevelopmental disorders. *Medical Image Analysis*, 90:102932, 2023.
- Cai Zhou, Xiyuan Wang, and Muhan Zhang. Facilitating graph neural networks with random walk on simplicial complexes. In A. Oh, T. Naumann, A. Globerson, K. Saenko, M. Hardt, and S. Levine, editors, *Proceedings of the 37th Neural Information Processing Systems*, pages 16172–16206, 2023.

A Additional Experiments

Due to page limitations, only the experimental results for the AUC metric are included in the main text. For a more comprehensive study, the full results of the comparison experiments are provided in this appendix.

Datasets. We preprocess the fMRI using the Data Processing Assistant for Resting-State Function (DPARSF) MRI toolkit. Specifically, we removed the first 10 time points from the downloaded nii data according to the default mode and chose slice timing, where the middle layer was the reference slice. meanwhile, we set the head motion correction to ‘Friston 24’, and selected automask and Nuisance covariates regression. the others were basically set according to the default mode. Then, considering individual differences, we choose to perform ‘Normalize by DARTEL’, and for the definition of ROIs, we adopt the atlas already available in DPARSF. Finally, we construct brain networks for each fMRI. For parcellation, we utilize the Craddock 200 atlas, which defines 200 ROIs, for the ABIDE dataset. For the ADNI dataset, we apply the AAL atlas, comprising 90 cortical ROIs and 26 cerebellar ROIs.

Baselines. The selected baselines correspond to two categories. The first category is generalized graph learning methods, including SAN Kreuzer et al. [2021], Graphormer Ying et al. [2021], GraphTrans Wu et al. [2021], and LRGNN Wei et al. [2023]. SAN and Graphormer are two more popular Transformer-based graph learning methods. GraphTrans is capable of capturing long-range dependencies within general graphs. LRGNN combines neural architecture search to extract the long-range dependencies. The second category is the brain graph-based methods, including BrainNetGNN Kan et al. [2022b], FBNETGEN Kan et al. [2022a], BrainGNN Li et al. [2021], BrainNETTF Kan et al. [2022b], A-GCL Zhang et al. [2023], and ContrastPool Xu et al. [2024]. BrainNetGNN utilized attention-based GNN to learn the representation of brain networks. FBNETGEN employed task-aware GNN, and BrainGNN adopted GNNs with ROI-aware and ROI-selection. BrainNETTF modeled a specific Transformer and readout function for brain network analysis. A-GCL utilizes adversarial graph contrastive learning to extract invariant features from brain networks. ContrastPool is capable of generating task-relevant, interpretable brain network representations. Although these methods show advantages in brain network analysis tasks, none of them analyzed and captured long-range dependencies within brain networks.

To ensure a fair comparison, we use the open-source codes of BrainGNN Li et al. [2021], BrainNETTF Kan et al. [2022b], FBNETGEN Kan et al. [2022a], A-GCL Zhang et al. [2023], and ContrastPool Xu et al. [2024]. For SAN Kreuzer et al. [2021], Graphormer Ying et al. [2021], LRGNN Wei et al. [2023], and GraphTrans Wu et al. [2021], we adapt their open-source codes and modify them to suit the brain network datasets. For BrainNetGNN, we implemente it ourselves following the settings described in the paper. During the parameter tuning, we follow the tuning of BrainNETTF Kan et al. [2022b] for SAN, BrainGNN, FBNETGEN, Graphormer, and BrainNETTF. For BrainNetGNN, we search the number of GRU layers 1, 2, 3. For LRGNN, we vary the aggregation operations 8, 12 with the number of cell 1, 3. For GraphTrans, we search the number of GNN layers 1, 2, 3, 4 with the hidden dimension of 100. Regarding the construction of brain graphs for these baselines, we utilized functional connectivity matrix to compute a brain graph for BrainNETTF, which is computed by calculating the correlation between brain ROIs using the processed fMRI. The details of computing these correlation matrices is also incorporated to the revised paper. For BrainNetGNN and FBNETGEN, the models required the processed fMRI as input. ContrastPool, A-GCL, BrainGNN, SAN, Graphormer, LRGNN, and GraphTrans required the correlation matrix and adjacency matrix. As mentioned in the paper, the adjacency matrix is obtained by thresholding (≥ 0.3) the correlation matrix.

Adaptive Long-range Aware with Varying Readout Functions. The full results of the ablation study on the three frameworks, VanillaTF, Graphormer, and SAN, are presented in Table 3, 4, and 5. Based on the results from the three tables, it is evident that, with the aid of the ALGA strategy, each framework employing various readout functions demonstrates superior performance across AUC, ACC, and SPE metrics. Furthermore, we observe that each framework based on clustering-based pooling exhibits significantly lower standard deviation in performance metrics when utilizing the ALGA strategy compared to those without it.

Table 3: Performance comparison with varying readout functions on the VanillaTF framework (%). The overall best results are highlighted in bold, while better results with/without ALGA are indicated by underlining. Standard deviations are presented in parentheses.

| Readout | w/o ALGA | | | | ALGA | | | |
|------------|-----------|-----------|-----------|-----------|-------------------------|-------------------------|-------------------------|-------------------------|
| | AUC | ACC | SEN | SPE | AUC | ACC | SEN | SPE |
| MEAN | 73.4(1.4) | 67.4(1.2) | 68.3(1.2) | 66.7(1.2) | <u>75.6(1.6)</u> | <u>71.6(1.3)</u> | <u>70.8(1.2)</u> | <u>69.4(1.2)</u> |
| MAX | 75.6(1.4) | 68.4(1.3) | 69.5(1.4) | 67.7(1.2) | <u>76.4(1.7)</u> | <u>72.6(1.4)</u> | <u>71.7(1.3)</u> | <u>70.7(1.1)</u> |
| SUM | 70.3(1.6) | 62.4(1.3) | 63.6(1.4) | 67.6(1.2) | <u>72.0(1.2)</u> | <u>68.3(1.3)</u> | <u>68.6(1.2)</u> | <u>67.5(1.3)</u> |
| SORT | 72.4(1.3) | 65.2(1.2) | 66.0(1.2) | 65.3(1.3) | <u>74.4(1.4)</u> | <u>69.8(1.2)</u> | <u>69.9(1.3)</u> | <u>69.1(1.2)</u> |
| CLUSTERING | 80.2(1.0) | 71.0(1.2) | 72.5(5.2) | 69.3(6.5) | <u>82.8(1.1)</u> | <u>77.0(1.0)</u> | <u>77.4(3.4)</u> | <u>76.6(4.6)</u> |

Table 4: Performance comparison with varying readout functions on the Graphormer framework (%). The overall best results are highlighted in bold, while better results with/without ALGA are indicated by underlining. Standard deviations are presented in parentheses.

| Readout | w/o ALGA | | | | ALGA | | | |
|------------|-----------|-----------|------------------|------------|-------------------------|-------------------------|--------------------------|--------------------------|
| | AUC | ACC | SEN | SPE | AUC | ACC | SEN | SPE |
| MEAN | 50.1(1.1) | 48.6(2.2) | 69.1(5.7) | 39.6(6.2) | <u>52.4(1.4)</u> | <u>51.8(1.4)</u> | <u>72.7(5.2)</u> | <u>43.6(4.4)</u> |
| MAX | 54.5(3.6) | 53.3(2.1) | 74.7(5.2) | 40.4(24.2) | <u>56.1(1.4)</u> | <u>55.8(1.3)</u> | <u>73.9(6.2)</u> | <u>43.9(14.5)</u> |
| SUM | 54.1(1.3) | 53.9(1.4) | <u>74.6(4.4)</u> | 39.7(12.2) | <u>55.7(1.6)</u> | <u>57.8(2.1)</u> | <u>73.3(5.2)</u> | <u>50.7(10.2)</u> |
| SORT | 50.5(4.7) | 49.6(5.2) | <u>76.5(6.4)</u> | 40.6(19.3) | <u>52.9(5.3)</u> | <u>53.9(5.4)</u> | <u>80.7(11.3)</u> | <u>44.6(9.3)</u> |
| CLUSTERING | 64.9(2.7) | 60.3(3.3) | 79.4(12.5) | 41.7(20.1) | <u>67.2(2.5)</u> | <u>64.1(1.9)</u> | <u>82.3(10.3)</u> | <u>45.9(12.7)</u> |

The Impact of Hops and Adaptive Factors. In Table 6 and 7, we present the results of four metrics under different hops and with/without adaptive factors. Based on the results from the both tables, we observe that the proposed method typically achieves better performance on AUC and ACC metrics when using adaptive factors. Besides, we observe that, across both datasets, the proposed method generally performs exceptionally well with a hop count of 16. Hence, we set the number of hop to 16 in our comparison experiments.

The Sensitivity of ALTER. We present experimental results on the ABIDE dataset for hop counts k ranging from 2 to 16 to analyze the sensitivity of ALTER. As shown in Table 8, we observe that as the number of hops increases, ALTER generally exhibits improved performance, achieving the best results at 16 hops. This indicates that our method is influenced by the number of hops k , as ALTER relies on random walk sampling to capture long-range dependencies. Additionally, this phenomenon demonstrates the capability of the proposed method to capture long-range dependencies.

The Cases of the ALTER. To further illustrate the ability of the proposed method to capture long-range dependencies within brain networks, we perform sample-level and group-level analyses, respectively. For the sample-level analysis, we present four additional cases in the Figure 5. From the Figure 5(d), we observe that despite being separated by 6 hops, ALTER is still able to capture the dependency between nodes 6 and 12. For the group-level analysis, we have computed the average across individuals to perform group-level analysis, as this approach aligns with the methodologies commonly adopted in similar studies Sarwar et al. [2021]. The average graph and the corresponding attention heatmap are illustrated in Figure 6(b)&(c) of the global response. We can observe that ALTER captures group-level long-distance dependence, but it is not very significant relative to the individual-level. This may be due to certain individual differences in patients, including age and gender, which can affect the brain-wide communication Zamani Esfahlani et al. [2022].

The Interpretability of ALTER. We use the SHAP model for interpretability analysis on the ADNI dataset. We calculate the SHAP values of the attention matrix. From the Figure 6(a), it can be observed that the hippocampal regions of AD cases have positive SHAP values and the Top-10 ROIs with the highest SHAP values are almost always correlated with ADNI prediction, which is generally consistent with the results in Qiu et al. [2022].

Table 5: Performance comparison with varying readout functions on the SAN framework (%). The overall best results are highlighted in bold, while better results with/without ALGA are indicated by underlining. Standard deviations are presented in parentheses.

| Readout | w/o ALGA | | | | ALGA | | | |
|------------|-----------|-----------|-----------|------------|------------------|------------------|------------------|------------------|
| | AUC | ACC | SEN | SPE | AUC | ACC | SEN | SPE |
| MEAN | 63.7(2.4) | 60.7(3.3) | 56.7(1.3) | 58.6(2.4) | 64.4(1.6) | 62.8(2.5) | 57.6(1.5) | 63.4(3.6) |
| MAX | 61.9(2.5) | 56.9(2.9) | 54.2(3.1) | 52.4(4.2) | 63.1(1.7) | 59.4(1.2) | 54.1(3.4) | 59.9(3.1) |
| SUM | 62.0(2.3) | 57.8(2.6) | 55.7(3.2) | 60.7(4.7) | 63.5(1.2) | 60.7(1.4) | 57.8(2.4) | 61.6(5.2) |
| SORT | 57.4(5.2) | 55.6(5.2) | 53.7(4.3) | 56.7(3.2) | 60.2(1.4) | 58.9(4.7) | 56.5(4.5) | 59.8(3.6) |
| CLUSTERING | 70.6(2.4) | 67.3(3.4) | 56.7(7.5) | 67.6(12.4) | <u>72.5(1.9)</u> | <u>67.8(3.1)</u> | <u>58.9(6.5)</u> | <u>70.8(4.1)</u> |

Table 6: The Impact of Hops and Adaptive Factors on the ABIDE dataset (%). The overall best results are highlighted in bold, while better results with/without adaptive factors are indicated by underlining. Standard deviations are presented in parentheses.

| Hops | w/o adaptive factors | | | | adaptive factors | | | |
|------|----------------------|-----------|-----------|-----------|------------------|------------------|------------------|------------------|
| | AUC | ACC | SEN | SPE | AUC | ACC | SEN | SPE |
| 2 | 76.6(3.9) | 69.0(2.5) | 70.1(3.5) | 69.2(5.1) | 78.7(3.9) | 72.0(2.0) | 71.9(3.1) | 72.2(3.1) |
| 4 | 77.4(3.1) | 71.0(3.0) | 72.5(2.5) | 71.1(4.5) | 79.1(2.4) | 73.0(2.5) | 73.2(1.9) | 72.9(3.8) |
| 8 | 78.9(2.2) | 73.0(2.0) | 74.2(2.9) | 75.4(5.9) | 80.4(1.9) | 72.0(4.0) | 75.6(2.1) | 74.8(5.6) |
| 16 | 81.2(2.6) | 75.0(1.5) | 75.8(3.1) | 75.1(4.2) | 82.8(1.1) | 77.0(1.0) | 77.4(3.4) | 76.6(4.6) |
| 32 | 78.8(1.9) | 74.0(1.2) | 76.4(2.2) | 73.8(5.9) | 79.6(2.1) | 75.0(1.3) | 76.3(2.7) | 74.3(5.1) |

B Further Discussion

Possible Negative Societal Impacts. Given that the research in this paper involves neurological disease diagnosis, it is essential to declare the potential negative societal impacts of this study, even though it is currently in the research phase and has not yet been applied in practice. Specifically, in the process of AI-assisted disease diagnosis, erroneous results are inevitable. Such errors can have severe consequences for patients and society. Therefore, in real-world medical diagnostic scenarios, the final decision should always rest with the physician’s diagnosis.

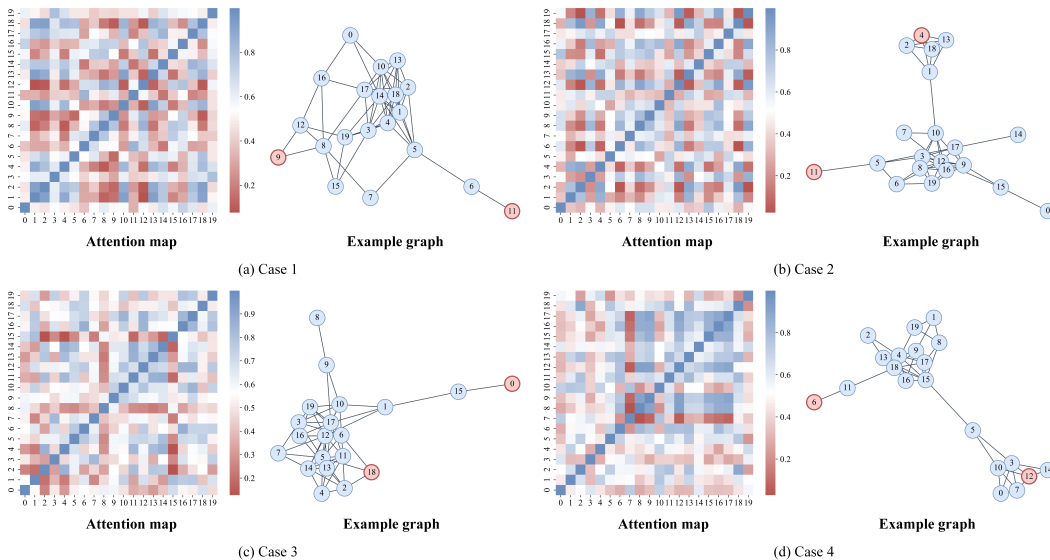


Figure 5: Example brain graphs from the ABIDE dataset and the corresponding attention heatmap.

Table 7: The Impact of Hops and Adaptive Factors on the ADNI dataset (%). The overall best results are highlighted in bold, while better results with/without adaptive factors are indicated by underlining. Standard deviations are presented in parentheses.

| Hops | w/o adaptive factors | | | | adaptive factors | | | |
|------|----------------------|-----------|-----------|------------------|-------------------|-------------------|-------------------|-----------|
| | AUC | ACC | SEN | SPE | AUC | ACC | SEN | SPE |
| 2 | 76.5(3.2) | 71.5(2.5) | 73.9(5.3) | 69.1(5.8) | 77.1(2.9) | 71.8(1.8) | 71.2(6.2) | 67.7(6.6) |
| 4 | 76.9(3.4) | 72.1(2.9) | 74.0(5.2) | 68.4(6.1) | 77.3(3.2) | 73.3(2.3) | 74.6(6.9) | 68.9(7.3) |
| 8 | 77.6(2.5) | 72.5(3.1) | 75.6(6.5) | 68.9(6.8) | 78.2(2.8) | 73.6(2.7) | 75.4(7.2) | 69.2(5.8) |
| 16 | 78.1(2.9) | 73.0(2.1) | 75.4(5.9) | 71.2(6.2) | 78.8 (2.1) | 74.1 (2.5) | 76.5 (6.1) | 70.0(6.5) |
| 32 | 76.2(2.9) | 73.0(1.2) | 74.0(4.5) | 70.7(5.5) | 77.9(2.6) | 73.5(2.6) | 74.9(5.2) | 70.3(6.1) |

Table 8: The sensitivity of ALTER on the ABIDE dataset. The best results are highlighted in bold, while standard deviations are presented in parentheses.

| Hops | ABIDE | | | |
|------|------------------|------------------|------------------|------------------|
| | AUC | ACC | SEN | SPE |
| 2 | 78.7(3.9) | 72.0(2.0) | 71.9(3.1) | 72.2(3.1) |
| 3 | 77.4(4.8) | 70.4(2.2) | 70.3(4.7) | 71.3(5.1) |
| 4 | 79.1(2.4) | 73.0(2.5) | 73.2(1.9) | 72.9(3.8) |
| 5 | 78.6(4.9) | 70.2(4.1) | 72.3(3.2) | 72.2(4.8) |
| 6 | 76.6(4.3) | 71.5(3.5) | 72.0(2.2) | 69.5(6.8) |
| 7 | 78.0(3.2) | 69.2(2.0) | 72.9(2.1) | 70.0(2.6) |
| 8 | 80.4(1.9) | 72.0(4.0) | 75.6(2.1) | 74.8(5.6) |
| 9 | 79.8(2.9) | 74.2(3.1) | 76.0(2.8) | 71.7(3.4) |
| 10 | 81.1(2.1) | 73.4(2.9) | 71.7(6.2) | 73.7(5.8) |
| 11 | 77.4(3.6) | 71.0(3.0) | 76.4(3.2) | 71.4(6.3) |
| 12 | 80.9(2.1) | 74.0(3.5) | 74.5(3.6) | 72.2(4.2) |
| 13 | 80.7(3.1) | 73.2(3.2) | 74.8(5.1) | 73.4(5.2) |
| 14 | 80.8(1.6) | 75.0(2.0) | 72.7(4.5) | 70.5(6.5) |
| 15 | 79.3(3.2) | 75.5(2.5) | 72.2(4.6) | 69.6(6.1) |
| 16 | 82.8(1.1) | 77.0(1.0) | 77.4(3.4) | 76.6(4.6) |

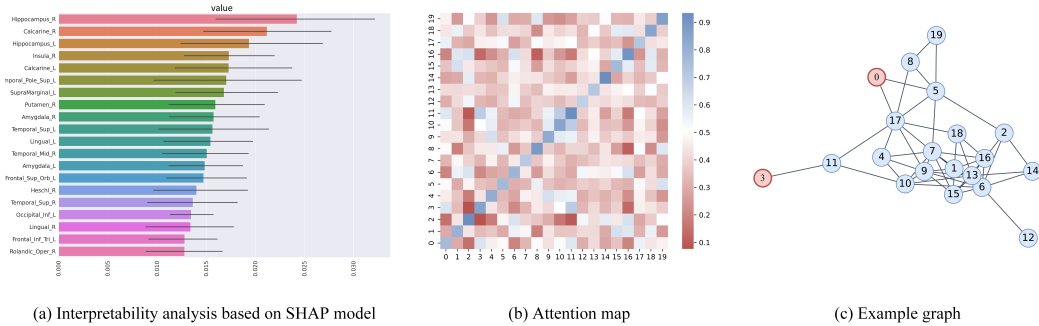


Figure 6: The interpretability analysis and group-level analysis.